Research Article | Vol. 30, No. 8 / 11 Apr 2022 / Optics Express 13469
Optics EXPRESS

Performance enhancement of solar cells based on high photoelectric conversion efficiency of h-BN and metal nanoparticles

JUN ZHU* AND GUANGMING JIN

College of Electronic Engineering, Guangxi Normal University, Guilin 541004, China
*zhujun1985@gxnu.edu.cn

Abstract: In this article, we propose a new type of CdTe thin-film solar cell based on a CdTe/CdS heterojunction. We used the finite difference time domain method to simulate the propagation of electromagnetic waves in the time domain under certain boundary conditions and the change in the absorption rate of cells when optimising the structure. The simulation shows that the light absorption rate of the cell is significantly enhanced after adding h-BN and metal particles to the proposed structure. Under the irradiation of standard light AM1.5 with the wavelength range of 300 nm to 1000 nm, presenting a 90% absorption bandwidth over 700 nm, and the average absorption rate is as high as 92.9%. The short-circuit current and open-circuit voltage are 30.98 mA/cm^2 and 1.155 V, respectively, and the photoelectric conversion efficiency (PCE) increases to 30.76%, which is an increase of 27.58% compared to the original PCE. The result shows that, after metal nanoparticles are embedded in the absorption layer of the cell, the free electrons on the surface of the metal particles oscillate under the action of light. The electromagnetic field is confined to a small area on the surface of the particles and is enhanced, which is beneficial for the absorption of light by the cells. This study provides a basis for theoretical research and feasible solutions for the manufacture of thin-film solar cells with a high absorption rate and high efficiency.

1. Introduction

In recent years, thin-film solar cells have received extensive attention and have been well researched due to their high absorption rate, flexible structure, and ease of manufacture [1,2]. Cadmium telluride (CdTe) is one of the most promising semiconductor materials for the manufacture of thin-film cells. It has a direct transition band structure, a spectral response that closely matches the solar spectrum, low bandgap (1.5 eV), high light absorption coefficient (>5×10^5 /cm), and other properties [3,4]. With the intensification of the environmental crisis [5,6], solar cells are now valued by all countries, and the development, research, and utilisation of solar photovoltaic materials have been raised to a strategic level. However, the high cost and low efficiency of traditional solar cells have severely restricted their development and widespread use [7,8]. Therefore, considerable research efforts are being made to improve the conversion efficiency of solar cells and manufacture high-performance and low-cost solar cells. To improve the light absorption rate of solar cells, various mechanisms have been proposed, including anti-reflection layers, grating structures, graphene heterojunctions, photonic crystals, and plasmonic nanoparticles [9–13]. The research group of Munday J N [14] proposed that the combination of plasmid grating and traditional AR coating can increase the short-circuit current to 1.8 times. Rassekh M et al. [15] studied the mechanism by which aluminium nanoparticles with different shapes enhance the light absorption rate of silicon thin-film solar cells. Their result showed that embedding aluminium particles in cells led to an increase in the absorption rate by more than 30%. J. Krügener et al. [16] proposed an inverted pyramid structure for photonic crystals to help reduce the thickness of the absorption layer, thereby minimising the inevitable internal

#453972 https://doi.org/10.1364/OE.453972
Journal © 2022 Received 17 Jan 2022; revised 10 Mar 2022; accepted 18 Mar 2022; published 6 Apr 2022

Optics EXPRESS

reorganization. Araujo A et al. [17] conducted experiments and observed that the photocurrent increased by 10.6% upon embedding silver nanoparticles in the absorption layer of the cells. Spyropoulos et al. [18] embedded Au nanoparticles into the photoactive material of the cell, and the PCE of the cell was enhanced by 40%. Li X et al. [19] inserted two-dimensional hexagonal boron nitride (h-BN) into the graphene / GaAs heterostructure, the barrier height of the heterostructure can be increased from 0.88 eV to 1.02 eV, thereby increasing the PCE of the cell from 8.63% to 10.18%. Jabeen M et al. [20] added h-BN interlayer in the silicon cell, which increased the short-circuit current of the cell by 6.2 mA/cm2, and the PCE increased from 10.93% to 12.03%. These methods reduced the reflection loss of light, increased barrier height, inhibited the transfer of electrostatic charge, and enhanced light absorption and current density. Although the structures and methods of these studies are relatively novel, the PCE of batteries is generally not high.

In this article, we propose a thin-film solar cell with CdTe/CdS as the PN heterojunction. We study the effects of h-BN, an etching indium tin oxide (ITO) grating structure, and embedded metal nanoparticles on the light absorption and photoelectric conversion efficiency (PCE) of the CdTe thin-film cell. We prove that in the visible light range, the absorption rate of CdTe thin-film solar cells remains above 90%, and the final PCE reaches 30.76%. Compared with traditional silicon solar cells, our proposed cadmium telluride thin-film solar cell not only has low cost and light weight, but also has a high absorption rate and good photovoltaic parameters.

2. Solar cell structure

2.1. CdTe thin-film solar cell

The XZ cross-section of the film structure proposed in this study is shown in Fig. 1. From top to bottom, the sequence is ITO/h-BN/CdS/CdTe (Au) /Al, and the geometric dimensions is shown in Table 1. The manufacturing process was as follows. First, the Al back electrode was cleaned, The 150 nm p-CdTe layer was deposited on the Al electrode, CdTe post-treatment (CdCl2 vapor phase annealing), the prepared Au NPs were deposited on 150 nm p-CdTe, and then 350 nm p-CdTe was electrodeposited to cover Au NPs, CdCl2 vapor phase annealing to process CdTe, and then the n-CdS layer was electrodeposited on the p-CdTe layer, h-BN layer and the ITO transparent conductive layer were thermally evaporated and deposited on the Al/CdTe/CdS, and then the ITO layer was etched into the grating structure. The ITO film is a transparent conductive film composed of a mixture of 90% In_2O_3 and 10% SnO_2 [21]. ITO has strong light transmittance and is often used in the top electrode of solar cells. To reduce the reflection of incident light, a layer of the ITO grating structure with a height of 30 nm and period of 80 nm was deposited on the surface of the cell. Hexagonal boron nitride is a two-dimensional dielectric material with good light transmittance and a high absorption coefficient. Its bandgap is 5.9 eV, and its dielectric constant is 4.0 [22]. We used 10-nm h-BN as the buffer layer of the cell to inhibit the transfer of static charge and reduce the carrier recombination velocity. The window layer of the cell was CdS with a thickness 50 nm, and the absorption layer was CdTe with a thickness 500 nm. CdTe and CdS formed a PN heterojunction. The band structure of the CdTe/CdS heterojunction is shown in the bottom right of Fig. 1. In addition, CdTe and CdS have large real refractive index and small imaginary refractive index in the wavelength range of 300nm-1000 nm, which is beneficial to the absorption of the cell. The mechanism of operation is as follows. After sunlight passes through the ITO and buffer layer, it is absorbed by the CdTe layer to generate electron-hole pairs. The electrons and holes are separated under the action of an electric field. The electrons deviate in the reverse direction and move through the CdS layer to the ITO front electrode. The holes move from the CdTe layer to the back electrode, thus generating current. Plasmonic Au nanoparticles with a radius of 100 nm and a period of 400 nm are embedded in the CdTe layer. The interaction of free electrons on the surface of the particles and photons from incident light can lead to electron oscillation, which is called localised surface plasmon resonance

Optics EXPRESS

(LSPR) [23,24]. An 80-nm-thick Al metal film was deposited on the bottom of the cell as the back electrode. It reduced the recombination of carriers on the back of the cell and increased the open-circuit voltage, thereby enhancing the reflection effect. The increase in the number of reflections and the optical path of light inside the cell improved the light absorption of the cell.

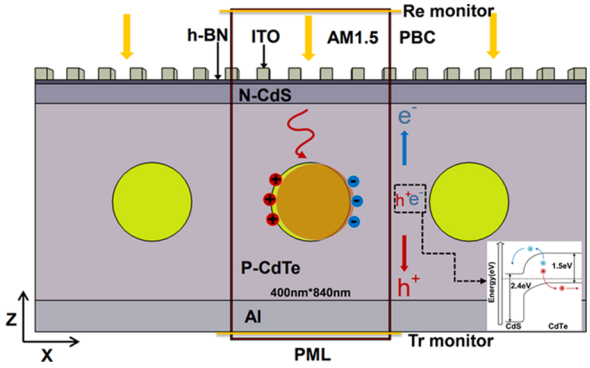

Fig. 1. XZ cross-section and working principle of CdTe thin-film solar cell.

Table 1. Dimensions and simulation parameters of solar cells

Material / Parameters	Size(nm)
ITO grating	h= 30 nm, p = 80nm
h-BN	h = 10nm
CdS	h = 50nm
CdTe	h = 500nm
Au nanoparticles	r = 100 nm, p = 400nm
Al	h = 80nm
Computational domain	400nm*840nm

2.2. Computation model analysis

We have used the finite difference time domain method for simulation calculations. The core idea is to calculate Maxwell's curl equation with the Yee cells discretization method [25], which can describe the propagation characteristics of the electromagnetic field more accurately. In the simulation, the X-axis is defined as the periodic boundary condition (PBC), and the upper and lower boundaries of the Z-axis are defined as the perfect matching layer (PML). To reduce the memory and time required for calculation, the simulation calculation range is one cycle, as shown in the yellow box in Fig. 1.

The X-axis width is 400 nm, the Z-axis height is 840 nm, the left and right sides of the domain are set as PBC, the upper and lower boundaries are defined as PML, and reflection and transmission monitors are placed above and below the computational domain. The absorption amount per unit volume is calculated by the divergence of the Poynting vector [26].

$$P_{abs} = -0.5Re(\overrightarrow{\nabla} \cdot \overrightarrow{S}) = -0.5\omega|\mathrm{E}(\omega)|^2 Im(\varepsilon(\omega)) \tag{1}$$

In the above equation, $\mathrm{E}(\omega)$ is the electric field intensity, and $\varepsilon(\omega)$ is the dielectric constant of the material. The ratio of the number of charge carriers absorbed by the solar cell to the number

Optics EXPRESS

of photons within a certain wavelength irradiated on the surface of the solar cell is defined as the quantum efficiency $QE(\lambda)$ of the solar cell [27].

$$\mathrm{QE}(\lambda) = \frac{\mathrm{P}_{abs}(\lambda)}{\mathrm{P}_{in}(\lambda)} \tag{2}$$

$P_{in}(\lambda)$ is the power of incident light, and the internal quantum efficiency of the solar cell is defined as follows [28].

$$IQE = \frac{\int \frac{\lambda}{hc} QE(\lambda) I_{AM1.5}(\lambda) d\lambda}{\int \frac{\lambda}{hc} I_{AM1.5}(\lambda) d\lambda} \tag{3}$$

In the above equation, h is the Planck constant, c is the speed of light, and $I_{AM1.5}$ denotes the $AM1.5$ solar spectrum. To study the effect of embedded metal particles on the solar cell, the enhancement factor of the internal quantum efficiency is defined as follows [29].

$$G = \frac{IQE_{particle}(\lambda)}{IQE_{reff}(\lambda)} \tag{4}$$

reff represents the reference cell (unoptimised cell), *particle* represents the cell embedded with metal nanoparticles.

To improve the light absorption of solar cells, metal particles are usually embedded in the absorption layer. Compared with other metallic materials, Au can excite a stronger coupling effect and lower ohmic loss, and it is not oxidised easily. Therefore, in this study, we have chosen gold as the research object. To explain the enhancement effect of Au nanoparticles on the cell, we studied the resonance of Au nanoparticles with a radius of 100 nm under the irradiation of incident light. Figure 2(a) shows the charge distribution on the surface of the gold particle. The free electrons of gold nanoparticles are displaced relative to the metal ion lattice. The electrons gather on the right and the holes move to the left. The resulting electric field is shown in Fig. 2(b). It exhibits evident dipole characteristics and the local field energy around the gold nanoparticles is enhanced by more than three times, which is conducive to the light absorption of the cell. When the dielectric constant of the metal is related to the frequency, the metal exhibits dispersion characteristics. In this study, the modified Drude model is used to calculate the dielectric constant of the metal, which is expressed as [30]:

$$\varepsilon_m(\omega) = \varepsilon_\infty - \frac{\omega_p^2}{\omega^2 - i\omega\gamma} \tag{5}$$

ω is the angular frequency of the incident light wave, $\omega_p = 1.37 \times 10^{16} rad/s$ is the plasma resonance frequency, and $\gamma = 4.08 \times 10^{13} rad/s$ is the plasma collision frequency [31].

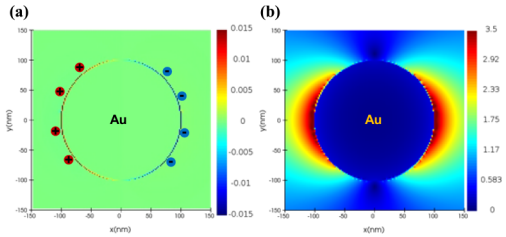

Fig. 2. (a) Charge around the Au particle with a radius of 100 nm. (b) Electric field diagram of the Au particle with a radius of 100 nm.

Optics EXPRESS

3. Calculation of optical properties

3.1. Analysis of absorption rate

To facilitate the analysis and comparison of the impact of each optimisation on the absorption rates of the solar cells, Fig. 3 shows the absorption rates of the CdTe thin-film solar cells at each occurrence of change in the structure. Figure 3(a) shows the reference cell with the unoptimised structure. The buffer layer of the reference cell is ZnO, and its bandgap is 3.2 eV. The blue line in Fig. 3 shows that in the wavelength range of 300 nm to 500 nm, the absorption rate of the reference cell is below 60%. Especially, at the wavelength of 300 nm, the absorption rate is only 24%. The structure in Fig. 3(b) replaces ZnO in the buffer layer with two-dimensional h-BN. The bandgap of h-BN is 5.9 eV, which can reduce the recombination rate of photogenerated carriers. The corresponding absorption rate is represented by the green line in Fig. 3. In the wavelength range of 300 nm to 540 nm, the absorption rate of the cell is enhanced. Particularly at the wavelength of 300 nm, the light absorption rate increases from 24% to 49.5%. However, the absorption rate decreases in the wavelength range of 540 nm to 730 nm. The absorption rate increases from 83.5% to 89% when the enhancement was maximum in the wavelength range of 730nm-1000 nm. In Fig. 3(c), ITO is etched into a periodic grating structure. The absorption rate of the cell with the grating structure is represented by the red line in Fig. 3. It is evident that the ITO grating structure increases the absorption rate of the cell by more than 85%. In Fig. 3(d), the plasmonic Au nanoparticle is embedded in the middle of the CdTe layer. After the Au particle is embedded, three absorption peaks appear at 350 nm, 625 nm, and 890 nm with absorption rates of 94.2%, 94.8%, and 97.0%, respectively. This shows that the optimised cell exhibits ultra-wideband light absorption. The average light absorption rate in the wavelength range of 300 nm to 1000 nm is as high as 92.9%.

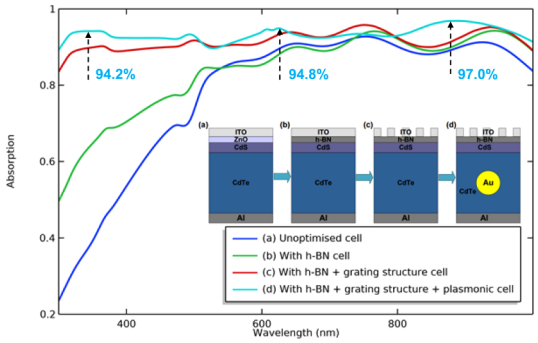

Fig. 3. Change in absorption rate of CdTe thin-film solar cells with different cell structures, where (a) reference cell, (b) cell with the buffer layer changed to h-BN, (c) cell with the grating structure, and (d) cell with metal nanoparticles.

To select the appropriate thickness of the h-BN film, we simulated the absorption rate of the cells with ZnO film or h-BN film as the buffer layers. As shown in Fig. 4(a), when the buffer layer is a h-BN film, the average absorption rate of the cell is increased from 53% to 70% in the wavelength range of 300 nm to 540 nm. Based on the overall absorption rate, the h-BN film is more suitable for the buffer layer of the cell than the ZnO film. In Fig. 4(a), the green and red lines are the absorption rates of the h-BN film with the thicknesses of 10 nm and 20 nm, respectively. In the wavelength ranges of 300 nm to 505 nm and 521 nm to 752 nm, the absorption rate of the h-BN film with a thickness of 10 nm is stronger than that of the h-BN film with a thickness of 20 nm. Therefore, the h-BN film with a thickness of 10 nm was finally selected as the buffer layer of the cell. As shown in Fig. 4(b) and Fig. 4(c), when the buffer layers of the cells are ZnO and h-BN, respectively, the charge diagrams at a wavelength of 300 nm show that the built-in electric

Optics EXPRESS

field splits the photogenerated carriers (electrons and holes) in two directions. Electrons are drawn to the n-CdS layer, and the holes drift to the back electrode [32]. Comparing the number of charges in the top layer in Fig. 4(b) and Fig. 4(c), it is observed that the h-BN layer has a stronger ability to collect photogenerated carriers than the ZnO layer because h-BN with a wide bandgap can effectively reduce the carrier recombination rate. To obtain the optimal height and period of the grating structure, we calculated the absorption rate of the ITO grating structure with different heights and different periods, as shown in Fig. 5(a). Irrespective of changing the height or period of the grating structure, absorption peaks appear at the same wavelength. According to the absorption rate, we selected the grating structure with a period of 80 nm and a thickness of 30 nm. The charge distributions without and with the ITO grating structure are shown in Fig. 5(b) and Fig. 5(c), respectively. It is observed that the carriers with the grating structure are layered distributed, which is due to the Fabry-Perot interference of incident light [33]. The result shows that as the grating structure is periodically and repeatedly arranged, the reflection loss of incident light decreases [34], and the pathlength of light increases due to multiple reflections. The grating structure ultimately enhances the light absorption of the solar cell.

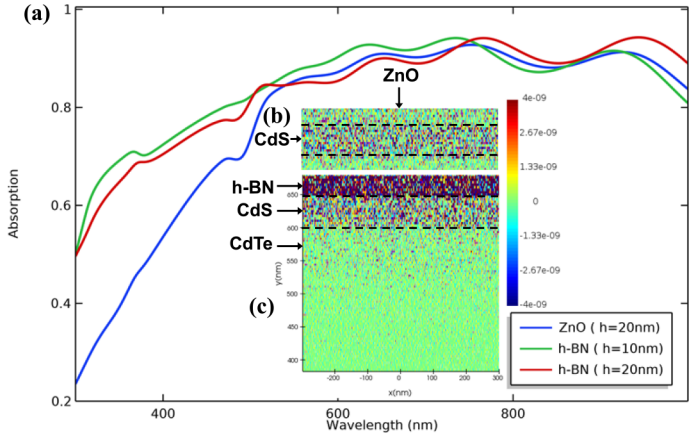

Fig. 4. (a) Absorption rate of solar cells with buffer layer of ZnO and h-BN. Charge distribution at a wavelength of 300 nm when the buffer layer is (b) ZnO, (c) h-BN.

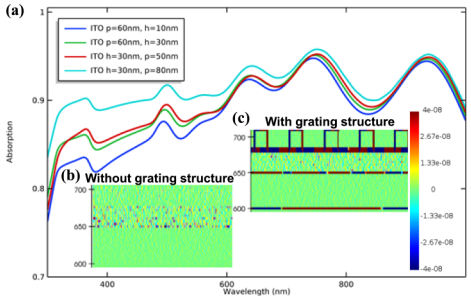

Fig. 5. (a) Absorption rate of ITO grating structures with different heights and different periods. (b) Charge distribution without ITO grating structure at a wavelength of 365 nm. (c) Charge distribution with ITO grating structure at the wavelength of 365 nm.

Optics EXPRESS

3.2. Comparative analysis of structures

We embedded plasmonic Au nanoparticles in the CdTe layer of the cells and compared the absorption rate of the cells before and after embedding Au nanoparticles with different radii. As shown in Fig. 6(a), between the wavelength of 300 nm and 510 nm, irrespective of the change in particle radius, there are two absorption peaks. When the radius of Au particles is 100 nm, the two absorption peaks are maximised, which are 94.2% and 93.5%, respectively. In the infrared wavelength range from 800 nm to 1000 nm, as the radius of Au particles increases, the absorption peaks have blue shifts and become steeper, indicating that the Au particles parasitically absorb the incident light. In the visible light wavelength range from 620 nm to 750 nm, Au particles with a radius of 120 nm have the lowest absorption rate. On one hand, parasitic absorption is evident, while on the other hand, for larger particle radius, more incident light is emitted back and cannot enter the absorption layer. Therefore, we have selected the radius of Au particles as 100 nm. In addition, we simulate and calculate the enhancement effect of the solar cell absorption when the metal particles are spaced differently, the result shows that when the spacing was 100 nm, because the spacing was too dense, part of the incident light was reflected without being completely incident on the absorber layer of the cell. When the spacing is 300 nm, the mutual coupling of free electrons on the surfaces of the two metal particles is weakened. Therefore, the spacing of the metal particles is finally selected to be 200 nm. To explore the mechanism of enhanced absorption of Au particles, we compared the electric field intensities before and after embedding Au nanoparticles at the absorption peak of 845 nm, as shown in Fig. 6(b) and Fig. 6(c). In Fig. 6(b), the electric field intensity in the absorption layer is layered distributed, which is caused by Fabry-Perot (F-P) interference of the incident light. In Fig. 6(c), the intensities of the electric field on both sides and above the Au particles are increased, which is mainly caused by the forward scattering effect of the Au particles on the incident light and the localised surface plasmon resonance around the Au particles. The increase in intensity enhances the light absorption of the cells. Studies have shown that the use of metal nanoparticles to enhance light absorption in thin-film solar cells is essential for achieving high-efficiency cells. Additionally, the result shows that the absorption energy is only enhanced on the surface of the Au particle, and the carrier does not enter the Au particle to cause loss. Therefore, the absorption is only in CdTe not absorbed in the Au and converted to the heat.

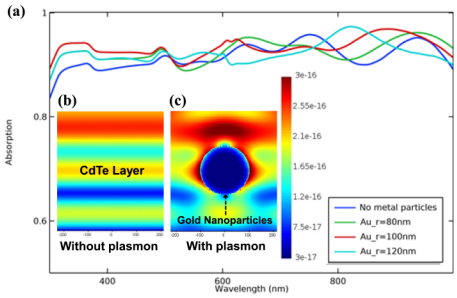

Fig. 6. (a) The absorption rate of the cells before and after embedding Au nanoparticles. Electric fields at a wavelength of 845 nm (b) before and (c) after embedding Au nanoparticles.

To further study the absorption rate of solar cells under sunlight, as well as the effect of each structural change on the absorption rate, we calculated the absorption spectrum under standard sunlight AM1.5. As shown in Fig. 7, the blue line represents the AM1.5 solar spectrum, UV (Ultraviolet) is the ultraviolet region, and IR (Infrared) is the near-infrared region. Figure 7 shows that adding h-BN and etching the ITO grating structure improves the light absorption of the solar cell in the wavelength range of 400 nm to 720 nm. The enhancement of light absorption after embedding Au nanoparticles is relatively small because the plasmonic Au particles on the

Optics EXPRESS

surface mainly act on long-wavelength photons, which have low spectrum energy [35]. After optimising the structure, the overall absorption rate of the cell is improved. The normalised average absorption spectrum in the visible light range of 380 nm to 780 nm accounts for 92.44% of the AM1.5 solar spectrum. An absorption rate of more than 90% is beneficial for the photoelectric conversion of solar cells.

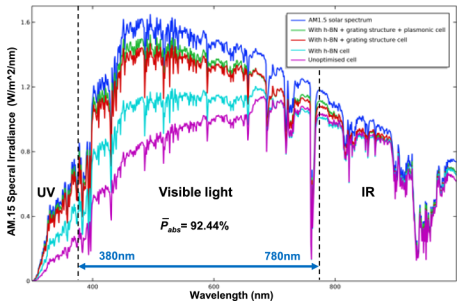

Fig. 7. Light absorption of CdTe thin-film solar cells under solar spectrum AM1.5.

4. Photovoltaic characteristics

4.1. Analysis of electrical characteristics

In this study, we have used CHARGE to analyse the electrical characteristics of the cell. Built on the finite element drift-diffusion method, CHARGE performs electrical simulations on data collected by optical simulations [36]. To measure the performance of solar cells, we define the following parameters. When the two ends of the solar cell are short-circuited, which means that the voltage is zero, the current flowing through the two ends of the solar cell is called the short-circuit current [37], which is defined as

$$J_{sc} = e \int \frac{\lambda}{hc} A(\lambda) I_{AM1.5}(\lambda) d\lambda \tag{6}$$

where e is an electronic charge ($e = 1.602 \times 10^{-19} C$), h is the Planck constant $h = (6.62 \times 10^{-34} J \cdot S)$, $I_{AM1.5}$ is the solar irradiance of the $AM1.5$ wide-band spectrum, and the range of λ is from 300 nm to 1000 nm. When the two ends of the solar cell are in an open circuit, which means that the current is zero, the output voltage at both ends is called the open-circuit voltage [38], which is defined as

$$V_{oc} = \frac{k_B T_a}{q} \ln\left(\frac{J_{sc}}{J_0} + 1\right) \tag{7}$$

where k_B is the Boltzmann constant which equals $1.380649 \times 10^{-23} J/K$, T_a is the ambient temperature, and J_0 is the reverse bias saturation current. We define the ratio of the maximum power of the solar cell to the ideal power as the fill factor, which is an important parameter for evaluating the output of the solar cell [39]. It is expressed as follows.

$$FF = \frac{P_{max}}{J_{sc} V_{oc}} \tag{8}$$

The ratio of the maximum output power P_{max} of the cell to the energy power P_{in} irradiated on the surface of the cell is defined as the PCE. The value of the PCE can directly reflect the characteristics of cell performance. The ultimate and most significant goal of researchers is to

Optics EXPRESS

improve the PCE η, which is defined as follows [20].

$$\eta = \frac{P_{max}}{P_{in}} = \frac{FF\ J_{sc}\ V_{oc}}{P_{in}} \tag{9}$$

Several parameters of the CdTe/CdS heterojunction are shown in Table 2. Standard incident light AM1.5 is used as the light source, and its energy density is 100 mW/cm^2. In addition to the absorption rate, the doping concentration of the PN junction is also very important for the overall photoelectric efficiency of the solar cell. An excessively high or overly low doping concentration can reduce the photoelectric efficiency of the solar cell. From the perspective of efficiency and process, the doping concentration of the P-type junction is 1×10^{19}, and the doping concentration of the N-type junction is 1×10^{17}. Figure 8 shows the J-V diagram and power diagram of the solar cell at each occurrence of change in structure, and it shows that each structural change can increase the current and voltage of the cell, especially after plasmonic Au nanoparticles are embedded. Due to the effect of surface plasmon, the enhancement of current is more observable, which increases by 1.47 $mA\ /\ cm^2$. After replacing the buffer layer with h-BN, h-BN reduces the recombination rate of carriers and increases the electron-hole pairs that drift to the two electrodes of the cell, thereby increasing the voltage across the cell.

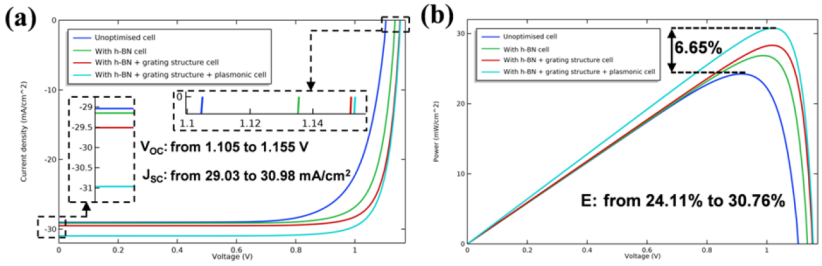

Fig. 8. (a) J-V diagram of CdTe thin-film solar cell. (b) Power diagram of CdTe thin-film solar cell.

Table 2. Several parameters of CdTe/CdS heterojunction.

Parameter	CdTe	CdS
Thickness (nm)	500	50
Bandgap energy, E_g (eV)	1.5	2.4
Electron affinity (eV)	4.28	4.2
Dielectric constant	9.4	10
Electrical conductivity (S/m)	2.154×10^{-9}	2.693×10^{-17}
Doping concentration (cm^{-3})	1×10^{19}	1×10^{17}

4.2. *Performance analysis of photovoltaic cell*

Table 3 shows the photovoltaic parameters of cells with different structures. It shows that after optimisation, the current, voltage, fill factor, and photoelectric efficiency of the cell are all improved. The PCE increases from 24.11% to 30.76%, which is an increase of 27.58%. The fill factor increases from 75.50% to 85.97%, which is an increase of 13.86%. The current and voltage increase by 5.06% and 4.5%, respectively. The PCE is an important factor for evaluating the quality of cells. In this study, we have increased the PCE of cells to more than 30%. This is a new breakthrough for improving solar cell technology, and it also makes it possible to use thin-film solar cells efficiently.

Optics EXPRESS

Table 3. Photovoltaic parameters of CdTe thin-film solar cells after each structural optimisation.

	$J_{sc}(mA\ /\ cm^2)$	$>V_{oc}(V)$	$FF(\%)$	$\eta(\%)$
Non optimised cell	29.03	1.105	75.16	24.11
With h-BN cell	29.15	1.136	80.68	26.72
With h-BN + grating structure cell	29.51	1.152	83.28	28.31
With h-BN + grating structure + plasmonic cell	30.98	1.155	85.97	30.76

Finally, the photovoltaic parameters of the CdTe thin-film solar cells proposed in this article are compared with the photovoltaic parameters of other similar thin-film solar cells in previous studies. The thickness and performance of thin-film solar cells with different structures are shown in Table 4. It is evident that the cell structure proposed in this article can significantly improve the short-circuit current, open-circuit voltage, and photovoltaic efficiency by reducing the carrier recombination loss and light reflection loss. Compared with previous studies [4], [40], and [41], the photovoltaic efficiency in this study is increased by 33.68%, 16.51%, and 8.27%, respectively. In addition, our proposed CdTe thin-film solar cell also has a huge advantage in terms of the thickness. Reducing the cell thickness to 0.67 um, not only reduces raw materials, but also reduces the cost of the cell.

Table 4. Photovoltaic parameters reported in previous studies.

Reference	Thickness (μm)	$J_{sc}(mA\ /\ cm^2)$	$V_{oc}(V)$	$FF(\%)$	$\eta(\%)$
[4]	6.6	29.09	0.95	83.47	23.01
[40]	1.7	29.57	1.026	86.96	26.40
[41]	1.2	28.74	1.15	86.03	28.41
This study	0.67	30.98	1.155	85.97	30.76

5. Conclusion

We propose a CdTe thin-film solar cell with an ITO grating structure and Au nanoparticles. Under certain boundary conditions, we solved the change in the absorption rate of the cell when h-BN was added to the CdTe thin-film solar cell, the ITO grating structure was etched, and metal nanoparticles were embedded. In the time domain, we simulated the propagation of electromagnetic waves and the physical process of their interaction with Au particles. By solving the differential equation system of the perturbation quantity, we calculated the absorption rate of the cell. We have verified that using h-BN as a buffer layer can inhibit electrostatic charge transfer, reduce carrier recombination loss, and significantly increase the light absorption of CdTe thin-film solar cells in the range of ultraviolet and visible light with wavelength from 300 nm to 540 nm. After etching the ITO grating structure and embedding metal nanoparticles in the cell, the absorption rate of the cell in the visible light range is finally increased to more than 90%, and the average absorption rate is as high as 92.9%.

The result of the photovoltaic performance analysis of the cells shows that after adding h-BN to the cells, etching the ITO grating structure, and embedding metal nanoparticles, the photovoltaic performance and PCE of the cells are significantly improved. After optimising the parameters, the current J_{sc}, voltage V_{oc}, fill factor FF, and the photoelectric efficiency η are 30.98 $mA\ /\ cm^2$, 1.155 V, 85.97%, and 30.76%, respectively. Finally, we verified that the proposed CdTe thin-film solar cell demonstrates high performance in terms of the absorption rate, absorption wideband, and photovoltaic efficiency. These results provide a reference for the industrial application of solar cells.

Optics EXPRESS

Funding. National Natural Science Foundation of China (51965007); Natural Science Foundation of Guangxi Province (2021GXNSFAA220013); Innovation Project of Guangxi Graduate Education (YCSW2022123).

Disclosures. No conflict of interest exits in the submission of this manuscript.

Data availability. Data underlying the results presented in this paper can be obtained from the authors upon reasonable request.

References

1. R. Tang, X. Wang, W. Lian, J. Huang, and T. Chen, "Hydrothermal deposition of antimony selenosulfide thin films enables solar cells with 10% efficiency[J]," Nat. Energy **5**(8), 587–595 (2020).
2. R. Lei H, X. Wang, and H. Zheng, "Design principles for plasmonic thin film GaAs solar cells with high absorption enhancement[J]," J. Appl. Phys. **112**(5), 054326 (2012).
3. X. Wu, "High-efficiency polycrystalline CdTe thin-film solar cells[J]," Sol. Energy **77**(6), 803–814 (2004).
4. E. Tinedert I, F. Pezzimenti, and L. Megherbi M, "Design and simulation of a high efficiency CdS/CdTe solar cell[J]," Optik **208**, 164112 (2020).
5. A. Hassan, Z. Ilyas S, A. Jalil, and Z. Ullah, "Monetization of the environmental damage caused by fossil fuels[J]," Environ. Sci. Pollut. Res. **28**(17), 21204–21211 (2021).
6. D. Huisingh, Z. Zhang, C. Moore J, Q. Qiao, and Q. Li, "Recent advances in carbon emissions reduction: policies, technologies, monitoring, assessment and modeling[J]," J. Cleaner Prod. **103**(Sep 15), 1–12 (2015).
7. K. Todorov T, M. Bishop D, and S. Lee Y, "Materials perspectives for next-generation low-cost tandem solar cells[J]," Solar Energy Materials and Solar Cells **180**, 350–357 (2018).
8. W. Chi and K. Banerjee S, "Progress in Materials Development for the Rapid Efficiency Advancement of Perovskite Solar Cells[J]," Small **16**(28), 1907531 (2020).
9. X. Liu, K. Cheng, P. Cui, H. Qi, and Z. Du, "Hybrid energy harvester with bi-functional nano-wrinkled anti-reflective PDMS film for enhancing energies conversion from sunlight and raindrops[J]," Nano Energy **66**(104188), 104188 (2019).
10. Y. Lili, X. Yimin, H. Yuge, and T. Junjie, "Investigation on the performance enhancement of silicon solar cells with an assembly grating structure[J]," Energy Convers. Manage. **54**(1), 30–37 (2012).
11. M. Yu, Y. Li, Q. Cheng, and S. Li, "Numerical simulation of graphene/GaAs heterojunction solar cells[J]," Sol. Energy **182**(APR.), 453–461 (2019).
12. W. Liu, H. Ma, and A. Walsh, "Advance in photonic crystal solar cells[J]," Renewable and Sustainable Energy Reviews **116**, 109436 (2019).
13. T H Meen, J K Tsai, S M Chao, and Y C Lin, "Surface plasma resonant effect of gold nanoparticles on the photoelectrodes of dye-sensitized solar cells[J]," Nanoscale Res Lett **8**(1), 450 (2013).
14. J N Munday and A Atwater H, "Large Integrated Absorption Enhancement in Plasmonic Solar Cells by Combining Metallic Gratings and Antireflection Coatings[J]," Nano Lett. **11**(6), 2195–2201 (2011).
15. M Rassekh, R Shirmohammadi, and R Ghasempour. Effect of plasmonic Aluminum nanoparticles shapes on optical absorption enhancement in silicon thin-film solar cells[J]. Physics Letters A, 2021.
16. J Krügener, M Rienäcker, and S Schäfer. Photonic crystals for highly efficient silicon single junction solar cells[J]. Solar Energy Materials and Solar Cells, 2021.
17. A. Araujo, J. Mendes M, and T. Mateus, "Ultra-fast plasmonic back reflectors production for light trapping in thin Si solar cells[J]," Sol. Energy **174**, 786–792 (2018).
18. D. Spyropoulos G, "Organic bulk heterojunction photovoltaic devices with surfactant-free Au nanoparticles embedded in the active layer[J]," Appl. Phys. Lett. **100**(21), 213904 (2012).
19. X Li, S Lin, and Xing Lin, "Graphene/h-BN/GaAs sandwich diode as solar cell and photodetector[J]," Opt. Express **24**(1), 134–145 (2016).
20. M Jabeen and S Haxha, "2D/3D graphene on h-BN interlayer-silicon solar cell with ZnO:Al buffer layer and enormous light captivation using Au/Ag NPs[J]," Opt. Express **28**(9), 12709–12728 (2020).
21. A. Valla, P. Carroy, F. Ozanne, and D. Muoz, "Understanding the role of mobility of ITO films for silicon heterojunction solar cell applications[J]," Solar Energy Materials and Solar Cells **157**, 874–880 (2016).
22. K K Kim, A Hsu, X Jia, and SM Kin, "Synthesis and characterization of hexagonal boron nitride film as a dielectric layer for graphene devices[J]," ACS Nano **6**(10), 8583–8590 (2012).
23. L. Qiao, W. Dan, L. Zuo, and Y. Ye, "Localized surface plasmon resonance enhanced organic solar cell with gold nanospheres[J]," Appl. Energy **88**(3), 848–852 (2011).
24. Z. Quaid, S. Jefferson, and P. Omar, "Two-color surface plasmon resonance nanosizer for gold nanoparticles[J]," Opt. Express **27**(3), 3200–3216 (2019).
25. D.M. Sullivan, *Electromagnetic Simulation Using the FDTD Method*. John Wiley & Sons (2013)
26. G Singh and S Verma S, "Plasmon enhanced light trapping in thin film GaAs solar cells by Al nanoparticle array[J]," Phys. Lett. A **383**(13), 1526–1530 (2019).
27. A Mohsin, M Mobashera, A Malik, and M Rubaiat, "Light trapping in thin-film solar cell to enhance the absorption efficiency using FDTD simulation[J]," J. Opt. **7**, 015019 (2020).
28. J. Yang W, Q. Ma Z, and X. Tang, "Internal quantum efficiency for solar cells[J]," Sol. Energy **82**(2), 106–110 (2008).

Optics EXPRESS

29. M. Rassekh, R. Shirmohammadi, R. Ghasempour, and F. R. Staraei, "Effect of plasmonic Aluminum nanoparticles shapes on optical absorption enhancement in silicon thin-film solar cells[J]," Phys. Lett. A **408**, 127509 (2021).
30. J Zhu and G Wang, "Measurement of Water Content in Heavy Oil with Cavity Resonator[J]," Results Phys. **18**, 103192 (2020).
31. X. Gu, R. Bai, J. Xing R, Z. Ying Q, and Y. Lee, "Ultra-narrow-band perfect absorber based on high-order plasmonic resonance in metamaterial[J]," J. Nonlinear Opt. Phys. Mater. **25**(01), 1650011 (2016).
32. J.-H. Meng, X. Liu, and W. Zhang X, "Interface engineering for highly efficient graphene-on-silicon Schottky junction solar cells by introducing a hexagonal boron nitride interlayer[J]," Nano Energy **28**, 44–50 (2016).
33. M. Long, Z. Chen, T. Zhang, Y. Xiao, and J. Xu, "Ultrathin efficient perovskite solar cells employing a periodic structure of a composite hole conductor for elevated plasmonic light harvesting and hole collection[J]," Nanoscale **8**(12), 6290–6299 (2016).
34. J. Zhang, Z. Yu, Y. Liu, H. Chai, J. Hao, and H. Ye, "Dual interface gratings design for absorption enhancement in thin crystalline silicon solar cells[J]," Opt. Commun. **399**, 62–67 (2017).
35. B. Shi, W. Wang, X. Yu, and L. Yang, "Enhancement of optical absorption in silicon thin-film solar cells with metal nanoparticles[J]," Opt. Eng. **56**(5), 057105 (2017).
36. M Riaz, K Earles S, A Kadhim, and A Azzahrani, "Computer analysis of microcrystalline silicon hetero-junction solar cell with lumerical FDTD/DEVICE[J]," Int. J. Comp. Mat. Sci. Eng. **06**(03), 1750017 (2017).
37. Q. Rehman, D. Khan A, D. Khan A, and M. Noman, "Super absorption of solar energy using a plasmonic nanoparticle based CdTe solar cell[J]," RSC Adv. **9**(59), 34207–34213 (2019).
38. B. Islam and H. Baghdad, "Simulation of Electrical Characteristics of PERC Solar Cells[J]," J. Electron. Mater. **47**(10), 5825–5832 (2018).
39. M. Leilaeioun and C. Holman Z, "Accuracy of expressions for the fill factor of a solar cell in terms of open-circuit voltage and ideality factor[J]," J. Appl. Phys. **120**(12), 123111 (2016).
40. K. Sobayel, M. Shahinuzzaman, N. Amin, M. R. Karim, and M. Akhtaruzzaman, "Efficiency enhancement of CIGS solar cell by WS2 as window layer through numerical modelling tool[J]," Sol. Energy **207**, 479–485 (2020).
41. S. Rahman and S. R. Al Ahmed, "Photovoltaic performance enhancement in CdTe thin-film heterojunction solar cell with Sb2S3 as hole transport layer[J]," Solar Energy **230**, 605–617 (2021).